Materials Transactions, Vol. 59, No. 9 (2018) pp. 1513 to 1519

Enhanced Mechanical Properties of Al–36Si Composite via Friction Stir Processing and Subsequent Heat Treatment

Chen Wang[1,2], Beibei Wang[2], Quanzhao Wang[2], Liqing Chen[1], Peng Xue[2,*], Bolv Xiao[2] and Zongyi Ma[2]

[1]*State Key Laboratory of Rolling and Automation, Northeastern University, 3-11 Wenhua Road, Shenyang 110819, China*
[2]*Shenyang National Laboratory for Materials Science, Institute of Metal Research, Chinese Academy of Sciences, 72 Wenhua Road, Shenyang 110016, China*

Friction stir processing (FSP) was applied to modify the microstructures of Al–36Si composite. FSP resulted in a significant breakup of coarse primary Si particles in the processed zone (PZ), and the size and aspect ratio of the Si particles decreased with increasing the number of FSP passes. The refinement and homogenization of Si particles during FSP can lead to an improvement in both strength and ductility, though FSP caused softening behavior in the PZ due to thermal cycle during the processing. Post-FSP aging treatment partially recovered the microhardness in the PZ of FSP samples, resulting in the enhanced strength and ductility. Furthermore, post-FSP T6 treatment resulted in a considerable enhancement in the microhardness in the PZ which could reach up to a similar level of the base material (BM). Therefore, the tensile strength was significantly improved to 381 MPa, which was much higher than that of the BM (187 MPa). This study provides an effective method of improving the mechanical properties of the Al–36Si composite. [doi:10.2320/matertrans.M2018090]

(Received March 14, 2018; Accepted June 26, 2018; Published August 3, 2018)

Keywords: *Al–Si composite, friction stir processing, heat treatment, microstructure, mechanical property*

1. Introduction

Al–Si composite exhibits very specific and interesting properties, such as low density, excellent wear resistance, superior corrosion resistance and low thermal expansion coefficient. Thus, they are widely applied in various industries, such as aerospace, automobile and electronic industries. Generally, increasing the content of Si element in the matrix will enhance the elasticity modulus and acquire better thermal performances. However, when the content of Si element is more than 30% (mass% was used for all the contents in this study) in the Al matrix, the inherent brittleness of the coarse primary Si particles can give rise to an extremely poor tensile properties. It is reported that an as-cast Al–30Si composite exhibited a very low tensile strength of only 50 MPa with an average Si particle size of 204 μm.[1)] Therefore, the extremely low strength and poor ductility inhibited the use of the Al–Si composite.

It is commonly believed that the poor tensile properties resulted from the brittleness of the coarse primary Si particles with irregular morphologies, the segregation of the Si particles, and the voids in the Al–Si interface and Al matrix.[2)] Consequently, the effective approaches to improve the mechanical properties of the Al–Si composite can be summarized as follows: refining the Si particles, redistributing the Si particles uniformly, as well as eliminating the voids.

In order to improve the mechanical property of the Al–Si composite, various techniques have been used to refine the primary Si particles, such as modifier treatment,[3,4)] spray forming melt modification,[5)] rapid solidification[6,7)] and equal channel angular pressing (ECAP).[8)] Zuo *et al.*[1)] studied the influence of complex modification process of P and Sr on the microstructure evolution of Al–30Si composite. After the addition of 2.0% Al–3P and 0.7% Al–10Sr master alloys which were continuously added during the melt inoculation and solidification process, the primary Si particles could be significantly refined from more than 200 μm to 32.8 μm with homogeneous distribution and the eutectic Si was obviously modified as fibrous simultaneously. Moreover, ECAP can lead to a significant refinement of the coarse Si particles by the severe plastic deformation. It is indicated that the equivalent diameter of the Si particles decreased from 19 μm to about 0.8 μm, and the corresponding tensile strength increased from 131 MPa to 176 MPa.[8)] However, these processes have a few limitations during practical application, such as relatively high cost, complicated processing steps, environmental pollution and the use of specific protecting atmospheres. Furthermore, these approaches cannot heal the casting voids effectively and redistribute the Si particles.

Recently, a new processing technique, friction stir processing (FSP), was developed for microstructure modification based on the basic principles of friction stir welding (FSW).[9,10)] It has been demonstrated that FSP can eliminate the voids effectively, refine the coarse reinforcement particles, and improve the microstructure homogeneity of discontinuous particles reinforced Al matrix composite by breaking up the coarse reinforcement particles and dispersing them into the Al matrix uniformly.[11,12)] Moreover, it is widely believed that multiple-pass FSP with a 100% overlap is an effective approach to achieve the microstructural refinement and homogeneity.[13)]

For Al–Si composite, FSP could generate uniformly distributed fine Si particles with an average size of 2.44 μm and an average aspect ratio of ~1.86, while the average size and aspect ratio of the original Si particles were 16.75 μm and 5.92, respectively. These microstructure changes lead to a remarkable improvement in both strength and ductility.[12)] Similarly, Rao *et al.*[14)] reported that FSP could reduce both the size and aspect ratio of the coarse Si particles in Al–30Si composite. These observations indicate that FSP should be an effective technique to modify the microstructure of Al–Si composite.

*Corresponding author, E-mail: pxue@imr.ac.cn

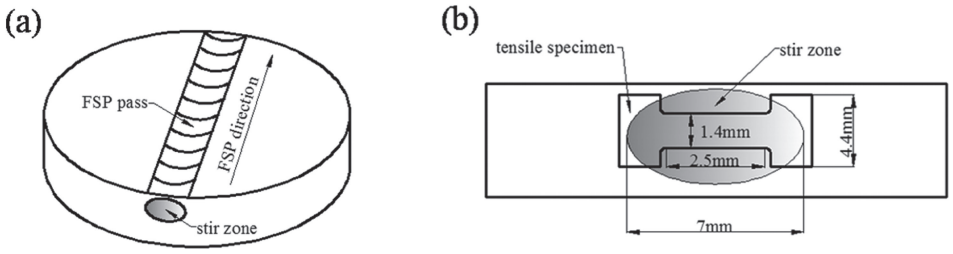

Fig. 1 Schematic illustration of (a) FSP process and (b) the location of the tensile specimen.

For age-hardened Al–Si composite, precipitates dissolution or coarsening in the matrix during FSP will lead to softening in the matrix. Therefore, a post-FSP heat treatment can be used to improve the mechanical properties.[12] For Al–6.5Si–0.35Mg composite, the tensile strength of the post-FSP artificially aged sample was ~40 MPa higher than that of the FSP sample.[15] However, the reinforcement effect was limited because post-FSP aging treatment did not exert a significant strengthening effect on an over-aged microstructure of as-FSP samples.[16] To further optimize the heat treatable Al matrix composites, post-FSP T6 (solution and artificial aging) treatment can be considered to achieve peak-aged microstructure.

Till now, very limited work has been performed to study the influence of FSP on the mechanical properties of Al–Si composite, especially for the high Si content. In this study, a typical Al–36Si composite (containing 1% Mg) was subjected to FSP with 1–4 passes, and post-FSP aging and post-FSP T6 treatment were performed. The aim is (a) to examine the effect of FSP passes on the microstructure and mechanical properties, (b) to enhance the mechanical properties of Al–36Si composite by post-FSP heat treatment, (c) to investigate the fracture mechanisms of various FSP samples.

2. Experiment

The initial work piece was produced by powder metallurgy method and then was forged into a disc plate with a diameter of 120 mm with a chemical composition of 36% Si, 1% Mg and balance Al. The forged disc plate was subsequently conducted to T6 treatment which was defined as the base material (BM). FSP was performed using a cermet tool with a concave shoulder diameter of 20 mm, and a threaded cylindric pin with a diameter of 8 mm and a length of 4.6 mm. FSP was conducted at a constant tool rotation rate of 2000 rpm and a traverse speed of 50 mm/min. The schematic illustration of FSP process is shown in Fig. 1(a).

In order to investigate the effect of FSP passes on the microstructure and mechanical properties of the Al–36Si composite, two-pass and four-pass FSP with 100% overlap on the processed zone (PZ) of the former pass were performed, and the samples were defined as 2-FSP and 4-FSP, respectively. During the multi-pass FSP experiments, each pass was performed after the work piece was fully cooled down to room temperature in order to avoid accumulative heating from the former pass of FSP. A subsequent artificial aging at 175°C for 4 h was performed on part of the FSP samples. Meanwhile, some samples were subjected to a T6 treatment (solution at 530°C for 0.5 h, water quenching and artificial aging at 175°C for 4 h). The PZs of as-FSP sample, aging-treated sample and T6-treated sample were defined as FSP, FSP-age, and FSP-T6, respectively.

The samples for microstructural investigations were machined perpendicular to the FSP direction. The specimens were ground and polished according to the standard metallographic procedures for the optical microscope (OM) observation, and subsequently observed on the OM and scanning electron microscope (SEM). The positions for calculated the average sizes of the Si particles for FSP samples were the top, middle, bottom, advancing side and retreating side of PZs, and the calculated size of each site was 0.4 mm × 0.3 mm which was chosen from four adjacent OM figures. The sizes of the Si particles in the PZs were estimated by Image-Pro software, and only particles with sizes of larger than 0.25 μm were brought into statistics, and an equivalent diameter d ($d = (d_L d_T)^{1/2}$) was used to define the size of the Si particles, where d_L and d_T were the dimensions of the major and minor axes of the particles, respectively. The aspect ratio of the Si particles was defined as the ratio of d_L to d_T.

Vickers hardness of the PZ was measured using a load of 1000 g for 15 s. Dog-bone shaped tensile specimens (2.5 mm gage length, 1.4 mm gage width, and 1.0 mm gage thickness) were electrical discharge machined perpendicular to the FSP direction with the gage part in the PZ, as schematically shown in Fig. 1(b). Tensile tests were conducted using an Instron 5848 micro-tester at an initial strain rate of $1 \times 10^{-3}\,s^{-1}$. The tensile property for each condition was obtained by averaging three testing results. After tensile tests, the fracture surfaces were examined by SEM and OM.

3. Results and Discussion

3.1 Microstructure evolution

Figure 2 shows a typical cross-sectional macrograph of Al–36Si composite after single pass FSP. It is noted that no defects were found in the FSP sample. Similar macrostructure was observed in other FSP samples including the samples after heat treatment. The PZ was made up of shoulder affected zone (SAZ) and pin affected zone (PAZ). The shape of the PZ was elliptical, which was related to the

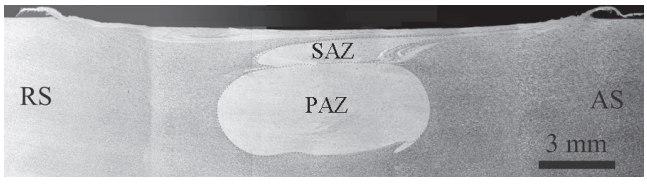

Fig. 2 Macrograph of single-pass FSP sample.

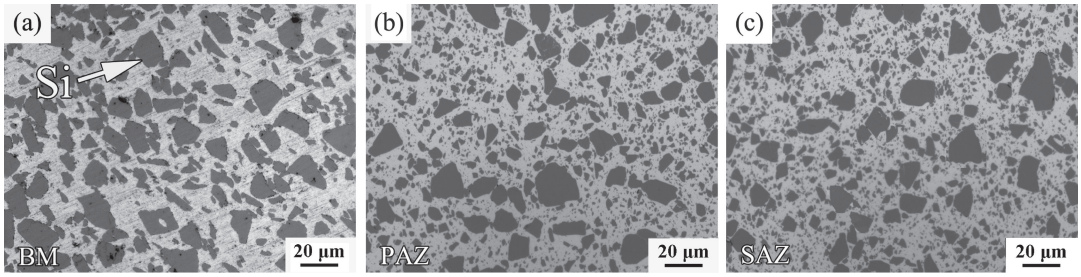

Fig. 3 OM micrographs in the BM and 1-FSP (a) BM, (b) pin region of PZ in Fig. 2, (c) shoulder region of PZ in Fig. 2.

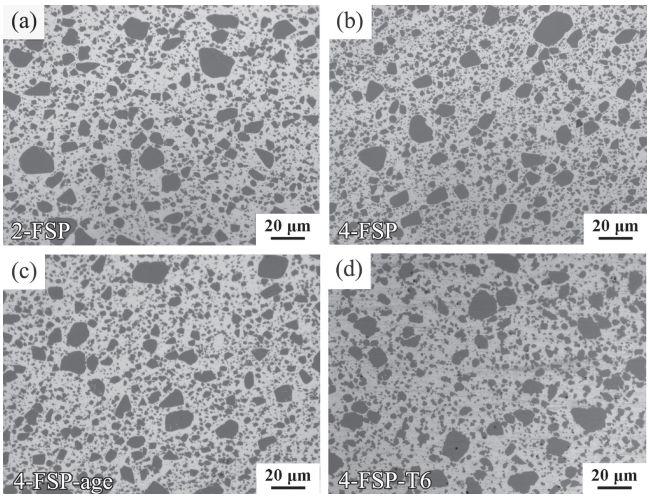

Fig. 4 OM micrographs in the samples of (a) 2-FSP, (b) 4-FSP, (c) 4-FSP-age, (d) 4-FSP-T6.

processing parameters, tool geometry, temperature, and thermal conductivity of the work piece.[17,18)]

Birol and Kasman[19)] indicated that the shape of the PZ was extremely affected by the pin profile rather than the welding parameters, a threaded cylindric pin created elliptical PZs while the basin-shaped PZs were produced by a triangular pin. However, Ma *et al.*[20)] found that higher tool rotation rate resulted in the generation of elliptical-shaped PZ, whereas the basin-shaped PZ was observed at a lower rotation rate. This suggested that varying processing parameters could produce different PZ shapes. In general, 2000 rpm is an extremely high rotation rate for the FSP of Al alloys and composites, and a threaded cylindric pin was used in this study, resulting in the formation of the elliptical PZ.

The typical microstructures of BM and FSP samples are shown in Fig. 3 and Fig. 4, and the calculated average sizes of the Si particles were shown in Table 1. Coarse primary Si particles were distributed throughout the Al matrix of the BM (Fig. 3(a)). Most Si particles are approximately equiaxed (the aspect ratio is about 2), with irregular shape and sharp corners. FSP resulted in a remarkable breakup of the coarse Si particles, and subsequently created a uniform redistribution of the broken Si particles in the Al matrix (Figs. 3(b) and (c)). As can be seen from Figs. 3(b) and (c), there was no distinct distinguish between the microstructure in the PAZ and that in the SAZ. Therefore, we just observed microstructure, calculated average sizes and tested mechanical properties in the PAZ of the following FSP samples. Figure 5 and Fig. 6 represented the particle size distribution and the

Table 1 Size of Si particles and mechanical properties of the BM and FSP samples.

Sample	UTS(MPa)	El (%)	Micro-hardness(HV)	Mean size of Si particles
BM	187 ± 93	<0.2	176	7.68
1-FSP-PAZ	281±2	1.3±0.3	104	2.87
1-FSP-SAZ	278±3	1.5±0.3	103	2.86
2-FSP	282±2	1.5±0.3	105	2.51
4-FSP	300±2	2.2±0.3	107	2.09
1-FSP-A	316±2	1.7±0.4	118	2.87
2-FSP-A	330±2	1.0±0.4	118	2.51
4-FSP-A	338±3	2.0±0.5	122	2.09
1-FSP-T6	249±1	<0.2	162	3.03
2-FSP-T6	324±4	<0.2	165	2.72
4-FSP-T6	381±5	<0.2	166	2.33

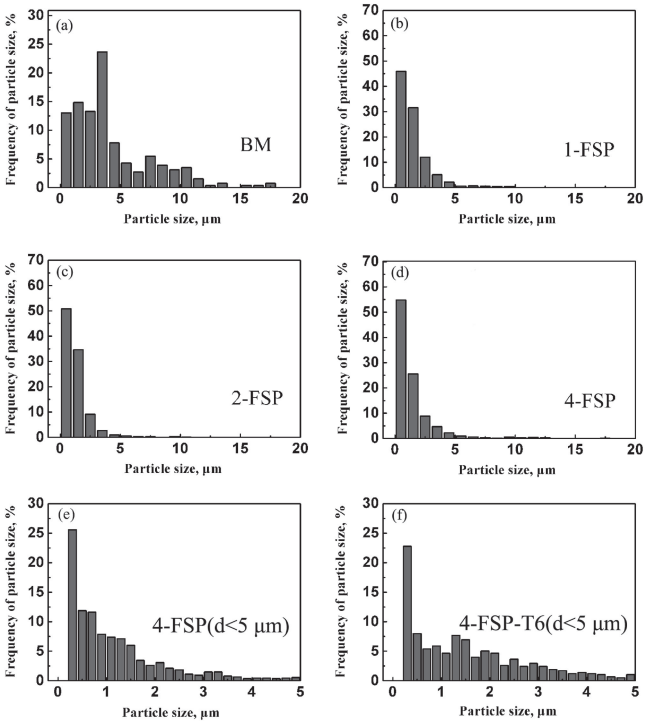

Fig. 5 Distribution of particle area against Si particle size in the samples of (a) BM, (b) 1-FSP, (c) 2-FSP, (d) 4-FSP, and more detailed distribution with the size smaller than 5 μm of (e) 4-FSP, (f) 4-FSP-T6 samples.

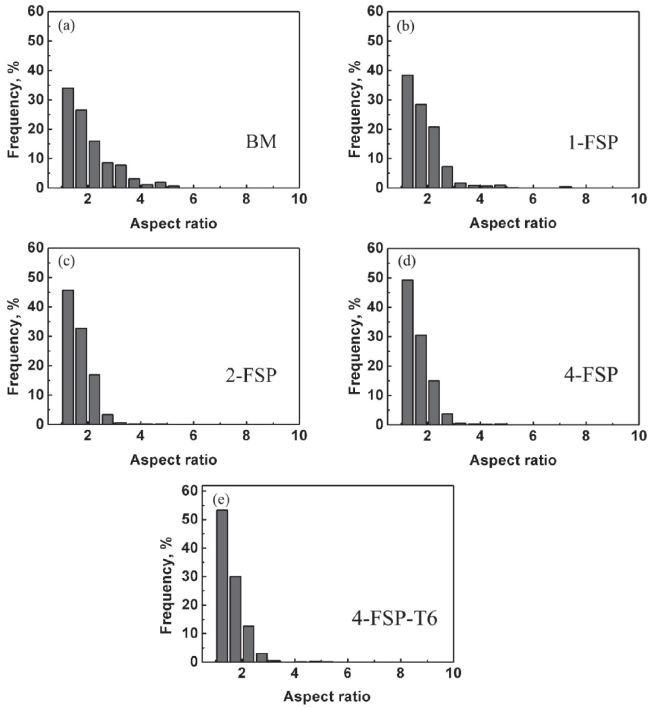

Fig. 6 Distribution of aspect ratio of Si particle in the samples of (a) BM, (b) 1-FSP, (c) 2-FSP, (d) 4-FSP, (e) 4-FSP-T6.

aspect ratio of the BM and FSP samples, respectively. The size of about 70% of the Si particles was less than 5 μm and the aspect ratio of about 60% of the particles was smaller than 2 in the BM. Meanwhile, many coarse Si particles with the size of larger than 5 μm could be observed and an average size of the Si particles was about 7.68 μm in the BM.

The average size of the Si particles decreased to 2.87 μm after one-pass FSP and further decreased with increasing the number of FSP passes, and an average size of 2.09 μm was achieved in 4-FSP sample (Table 1). Different from the BM, the size of most particles in the FSP samples was less than 5 μm and the particles always exhibited approximately equiaxed state (the aspect ratio is <2). However, some coarse Si particles still existed in the FSP samples even after 4 passes. During FSP, the material in the PZ underwent intense plastic deformation and thermal exposure. It is estimated that one-pass FSP could produce an effective strain of larger than 40.[21] Due to the intense plastic deformation and mixing during FSP, many larger Si particles in the PZ were broken up; meanwhile, the rotating pin also eliminated the corners and sharp edges of the large Si particles, blunting the sharp Si particles.[22]

Compared to the FSP sample, post-FSP aging treatment did not alter the dispersion of Si particles (Fig. 4(c)), but post-FSP T6 treatment coarsened and rounded the Si particles especially for the dispersed fine Si particles (Fig. 4(d)). To observe the change in the fine Si particles more distinctly after T6 treatment, the distribution of the fine Si particle size ($d < 5\,\mu m$) were further analyzed, as shown in Fig. 5(e) and (f). Post-FSP T6 treatment led to a quantitative reduction of the dispersed fine Si particles ($d < 1\,\mu m$) from 57% to 40% for four-pass FSP samples. Besides, T6 treatment also caused spheroidization of the broken Si particles to a certain extent (Fig. 6(d) and (e)).

3.2 Micro-hardness

The micro-hardness values of the PZs produced by FSP and subsequent heat treatments are summarized in Table 1. For 1-FSP sample, the micro-hardness value of SAZ is nearly similar with that of PAZ. Compared to the BM (176 HV), the micro-hardness value in the PZ decreased to 103–107 HV after FSP. After aging at 175°C for 4 h, the micro-hardness value in the PZ increased to 118–122 HV. It is worth mentioning that the micro-hardness in the PZ increased further to 162–166 HV after T6 treatment, which reached to the similar micro-hardness to that of the BM. This suggested that post-FSP heat treatment could improve the micro-hardness in the PZ due to the formation of the precipitates. Meanwhile, it is observed that increasing FSP passes had no significant effect on the micro-hardness in the PZ, but there was still an elevating trend in the micro-hardness as the FSP passes increased.

Softening in the PZ is mainly related to the dissolution and/or coarsening of the fine needle-shaped β'' precipitates which are the main hardening and strengthening source of the BM, due to the frictional heating and intense plastic deformation during FSP.[23] Bratland *et al.*[24] reported that the solution temperature of β-Mg_2Si is about 518°C in Al–Mg–Si alloys, and both β' and β'' precipitates have a much lower solution temperature. Cui *et al.*[25] has proven that the peak temperature during FSP could reach up to above 540°C. Therefore, it is possible that all or most of the precipitates in the PZ were dissolved in the Al matrix rapidly during the FSP thermal cycles.

Sato *et al.*[23] reported that there were no any precipitates in the PZ during FSW of 6063 Al alloy. Differently, El-Rayes and El-Danaf[26] found that the coarsening of precipitates from needle-shape β'' phase into semi- and non-coherent rod-shaped β' phase occurred in the PZ during FSP of 6082-T651 Al alloy. Although the peak temperature in the PZ was high enough to dissolve all the precipitates, the supersaturated solutes was not quenched but cooled slowly in air after FSP. Cui *et al.*[25] reported that the cooling process in PZ endured more than 200 seconds from peak temperature to room temperature. This should lead to re-precipitation of β'' precipitates during the slow cooling process, then subsequently coarsened into β' phase and even to β phase, resulting in an over-aged microstructure.

Assume that the precipitates in the PZ were completely dissolved in the Al matrix, it is expected that the subsequent artificial aging treatment could significantly improve the micro-hardness due to the re-precipitation effect. However, the micro-hardness in the PZs of FSP samples only recovered a little after artificial aging treatment, but exhibited a considerable reduction compared with that of the BM (Table 1). This confirmed that mainly over-aged microstructure (β' or β precipitates) was obtained in the Al matrix after FSP, because subsequent artificial aging treatment exerted no significant hardening effect on the over-aged microstructure. Consequently, the material softening should be mainly related to the coarsening of the precipitates in the PZs.

3.3 Tensile properties and fracture behavior

The tensile properties of the BM and various FSP samples were summarized in Table 1. The BM exhibited a rather wide range of ultimate tensile strength (UTS) of 187 ± 93 MPa

with a poor ductility (El. < 0.2%). As shown in Fig. 3(a), the BM consisted of many coarse primary Si particles which tended to crack earlier during tensile deformation, resulting in a reduction in both strength and ductility. Furthermore, cracks may also initiate at the structural defects such as the voids in the Al matrix or at the Al–Si interfaces.[27] Therefore, the present BM exhibited low strength and ductility.

It is clear that all the FSP samples exhibited higher UTS though a reduced hardness was achieved compared with that of the BM, and the ductility was significantly improved. Meanwhile, the PAZ exhibited the similar UTS with SAZ in the PZ. The improvement in the tensile properties after FSP should be attributed to the significant microstructural refinement, homogenization, and densification.[28] First, the breakup of the coarse primary Si particles significantly reduced the cracking tendency from the Si particle under low stress. Second, a uniform distribution of the broken Si particles also contributed to the improvement of the strength and ductility. Third, the elimination of the voids reduced the possibility of preferential crack initiation. Finally, the grain size of the Al matrix should be decreased after FSP compared to that of the BM, which was beneficial to the improvement of the mechanical properties.[9,10] Furthermore, both the strength and elongation increased slightly with increasing the number of FSP passes. A high UTS of 300 MPa was obtained in the 4-FSP sample with an enhanced elongation of 2.2%. This should be attributed to the further grain refining of the Al matrix and the reduced size of the Si particles with increasing the FSP passes.

Post-FSP aging treatment resulted in a further increase in the strength but had no significant effect on the elongation compared with the FSP samples. For example the UTS increased to 338 MPa for 4-FSP-age sample and the elongation slightly reduced to 2.0% compared to that of 4-FSP sample. Generally, for the Al–Si composite, the variation of the tensile properties should be affected by the Si particles and precipitates in the Al matrix. Although post-FSP aging treatment is hard to alter the morphology and distribution of Si particles, precipitation of more solutes in the aging process resulted in a further increase in the strength. However, the precipitates in the PZ cannot completely disappear after FSP because of the slow cooling rate in the air. Therefore, subsequent aging treatment probably gave rise to the coarsening of the original precipitates,[27] suggesting that post-FSP aging treatment has a limited improvement in the strength of the FSP samples.

To further enhance the strength, post-FSP T6 treatment could be an effective method of obtaining a peak-aging microstructure. Different from the BM with T6 treatment, the FSP-T6 samples exhibited much higher and more stable UTS due to the microstructural restructuring in the FSP process. The UTS of 4-FSP-T6 sample reached up to 381 MPa, which increased about 200 MPa compared with that of the BM. More importantly, the fluctuation of the UTS was only 5 MPa, which was greatly reduced than that of the BM (93 MPa). The significant enhancement in value and stability of the tensile strength should be attributed to the refinement and homogenization of Si particles during FSP and the spheroidization of Si particles in the subsequent T6 treatment, which reduced the probability of crack initiation during deformation and gave an additional improvement in strength.[29]

However, compared with 1-FSP sample, 1-FSP-T6 sample exhibited a lower UTS, which was contrary to the hardness results. The reason of the reduced strength was likely to be related to the no sufficient refinement of Si particles for only one pass of FSP, and resulting in the formation of irregular and coarsened Si particles after solution treatment under high temperature. To observe the Si particle coarsening more clearly, longer solution time (530°C for 1 h) were conducted on the 1-FSP sample. From the microstructure of the Si particles as shown in Fig. 7, obvious particle coarsening was observed after solution treatment for 1 h. Generally, the Si particles growing process can be summarized in Fig. 7(c). First, several adjacent fine Si particles moved together at the same time or fine Si particles moved toward the adjacent large particles under high temperature. When they closed enough to each other, these fine particles coalesced to an irregular-shaped large particle. Finally, the irregular-shaped particles tended to be rounded as the particles moved ceaselessly to a thermodynamical equilibrium state. The phenomenon of Si particles growth under the high temperature was also observed by Kliauga *et al.*[30] For 1-FSP-T6 sample with smaller solution time (0.5 h), the residual irregular-shaped particle with large size was prone to crack initiation and then resulted in a lower UTS during tensile process. Nevertheless, the 4-FSP-T6 sample exhibited more regular and round Si particles than 1-FSP-T6 sample, thereby resulting in the higher UTS.

Figure 8 shows the microstructure of the fracture surfaces for various Al–Si composites. The appearance of fracture surface confirmed the cleavage fracture mode in the BM which hardly contained any dimples (Fig. 8(a)), resulting in the low ductility. On a microscopic scale, the fracture surface appeared to contain many microcracks in the large Si particles. In case of FSP sample and FSP-age sample, although microcracks were observed at the coarse Si particles, plenty of dimples on the fracture surface generally gave the indication of significant improvement of ductility (Figs. 8(b) and (c)). Similar cleavage surface feature to that of the BM was also observed in the FSP-T6 samples, but the size of the Si particle was reduced and some ductile fractured characteristic could be observed (Fig. 8(d)).

Obviously, the improvement in ductility of the FSP samples was mainly attributed to the refinement and homogenization of Si particles. However, two kinds of post-FSP heat treated samples presented two different fracture mechanisms. The fractured specimens after tensile tests with the post-FSP aged and T6 treatment were examined by the OM. The FSP-age sample exhibited obvious necking behavior, showing a good ductility (Fig. 9(a)). However, no obvious necking phenomenon was observed from the FSP-T6 sample shown in Fig. 9(c), indicating a brittle fracture mode. For the Al–Si composite, cracks usually initiated preferentially at the coarse Si particles or the interface between the Si particle and Al matrix, due to the brittle nature of the Si particle and the incompatibility between the Si particle and Al matrix (Figs. 9(b) and (d)).[31] Then the cracks propagated through the coarse Si particles or along the Al–Si interface, and finally propagated into the Al matrix to failure during tensile deformation.

For the FSP and FSP-age samples, the refinement and homogenization of the Si particles greatly reduced the early

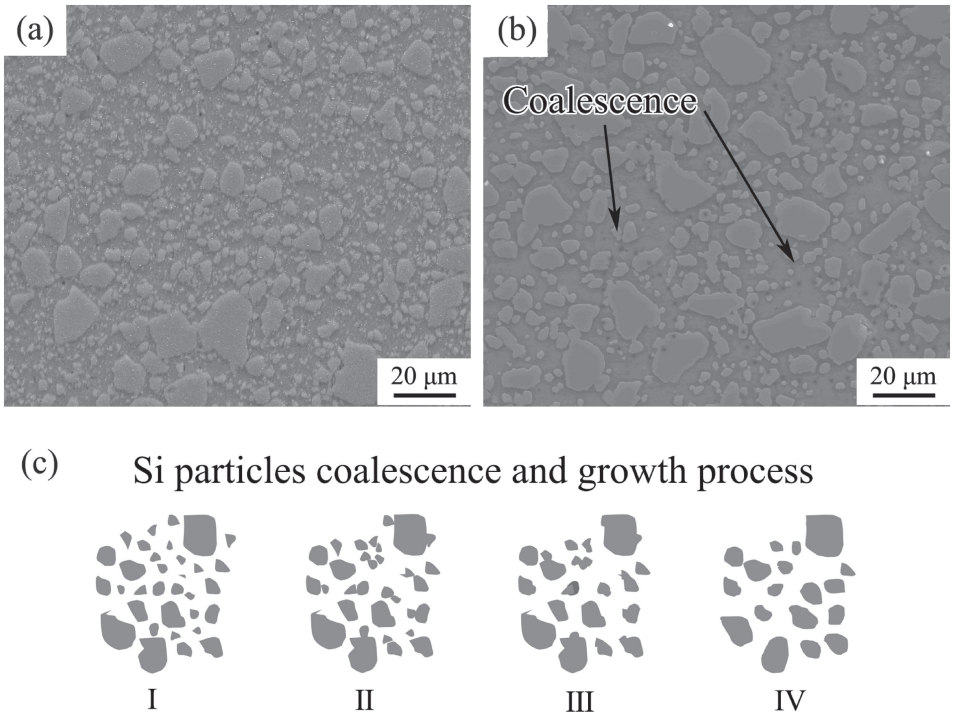

Fig. 7 SEM micrographs in the samples of (a) 1-FSP, (b) 1-FSP after solution treatment for 1 h, (c) schematic illustration of the Si particle coalescence and growth process.

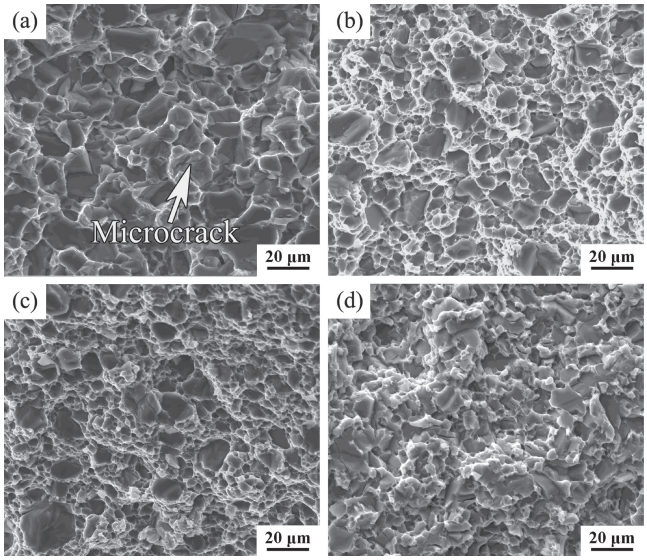

Fig. 8 SEM micrographs of fracture surfaces in samples of (a) BM, (b) 4-FSP, (c) 4-FSP-age, (d) 4-FSP-T6.

initiation tendency of the cracks, and crack propagation could be inhibited due to the enhanced property of Al matrix after FSP. However, for the FSP-T6 sample, the size of the large Si particle increased further, and the smaller Si particles grew and gathered in the Al matrix, resulting in the easier crack initiation. More importantly, severe stress concentration should exist at the coarse Si particle and the interface between the Si particle and Al matrix, which resulted from the high temperature solution treatment.[32] Therefore, the cracks easily initiated at the coarse Si particle and the interface between the Si particle and Al matrix, and propagated quickly into the matrix. In this case, brittle fracture was achieved in the FSP-T6 sample, but the strength and stability were significantly enhanced compared to the BM due to the refinement and homogenization of the Si particles.

4. Conclusions

In this study, the Al–36Si composite was subjected to FSP and post heat treatment, and the influence of FSP passes, post-FSP aging and T6 treatment on microstructure and mechanical properties were investigated. The conclusions are drawn from the present study as follows:

(1) FSP resulted in the significant breakup of coarse Si particles and created a redistribution of Si particles in the Al matrix, and the average size of Si particle decreased from 7.68 μm to 2.87 μm after FSP.

(2) Increasing the number of FSP passes led to a decrease in the average size and aspect ratio of the Si particles. The average size of Si particles reduced from 2.87 μm to 2.09 μm as the FSP pass increased from 1 to 4. Post-FSP aging treatment cannot change the size and distribution of Si particles, but post-FSP T6 treatment coarsened the fine Si particles, and rounded the corners and edges of the Si particles.

(3) The microhardness in the PZs decreased remarkably in FSP samples due to the dissolution and coarsening of precipitates under the thermal cycle during FSP. The number of FSP passes had no significant influence on the hardness. The subsequent aging treatment recovered the microhardness partly, while the subsequent T6 treatment significantly enhanced the microhardness up to the BM level.

(4) FSP resulted in a remarkable improvement in the tensile property of Al–Si composite, particularly in the ductility. The tensile strength and ductility increased with increasing the FSP passes, and a high UTS of

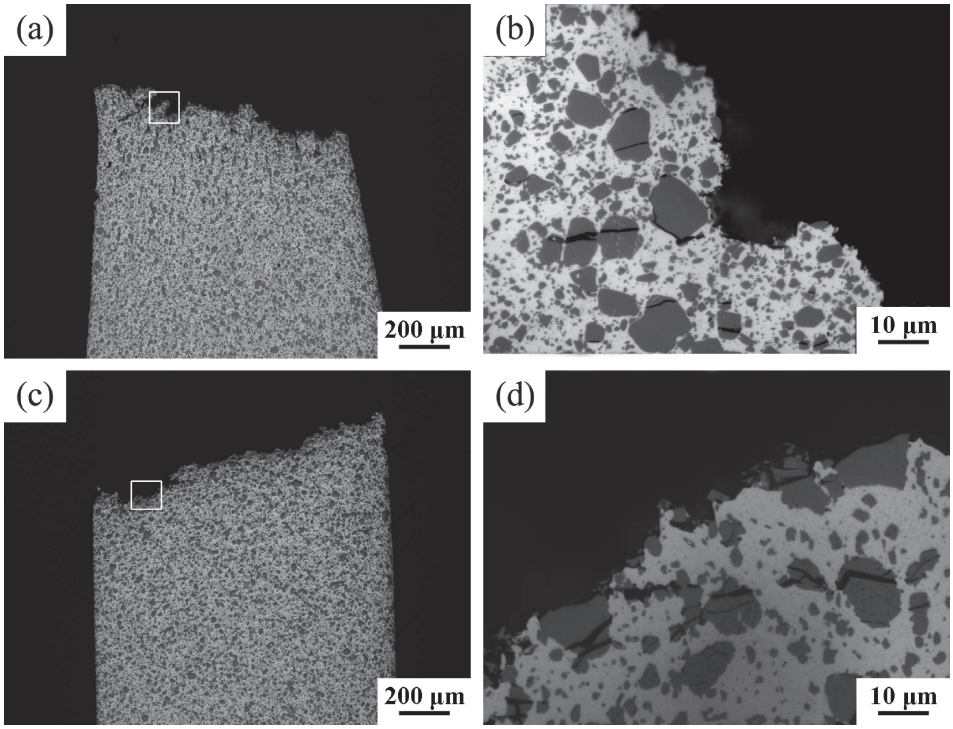

Fig. 9 Longitudinal fracture surface with different magnifications in the samples of (a) and (b) 4-FSP-age, (c) and (d) 4-FSP-T6.

300 MPa together with an enhanced ductility of 2.2% were achieved in 4-FSP sample. Post-FSP aging treatment further enhanced the tensile strength almost without losing the ductility. Post-FSP T6 treatment resulted in a significant decrease in ductility, but the highest tensile strength of 381 MPa was obtained in 4-FSP-T6 sample, which was much higher than that of the BM (187 MPa). Furthermore, a much reduced strength fluctuation of only 5 MPa was achieved in 4-FSP-T6 sample compared with that of BM (93 MPa).

Acknowledgments

This work was supported by the National Key R&D Program of China under grant No. 2017YFB0703104 and the National Natural Science Foundation of China under grant No. 51331008.

REFERENCES

1) M. Zuo, D.G. Zhao, X.Y. Teng, H.R. Geng and Z.S. Zhang: Mater. Des. **47** (2013) 857–864.
2) M.E. Seniw, J.G. Conley and M.E. Fine: Mater. Sci. Eng. A **285** (2000) 43–48.
3) H.C. Liao, K. Ding, J.J. Bi, M. Zhang, H.P. Wang and L. Zhao: J. Mater. Sci. Technol. **25** (2009) 437–440.
4) A. Bjurenstedt, S. Seifeddine and A.E.W. Jarfors: Metals **6** (2016) 1–15.
5) Y.D. Jia, F.Y. Cao, S. Scudino, P. Ma, H.C. Li and L. Yu: Mater. Des. **57** (2014) 585–591.
6) S.J. Hong: Mater. Trans. **51** (2010) 1055–1058.
7) S. Lee, B. Kim and S. Lee: Mater. Trans. **52** (2011) 1308–1315.
8) K.R. Cardoso, M.A. Muñoz-Morris, K.V. León and D.G. Morris: Mater. Sci. Eng. A **587** (2013) 387–396.
9) Y.G. Kim, I.J. Kim, Y.P. Kim and S.M. Joo: Mater. Trans. **57** (2016) 988–994.
10) K. Zhao, Z.Y. Liu, B.L. Xiao and Z.Y. Ma: J. Mater. Sci. Technol. **33** (2017) 1004–1008.
11) E. Meisam, M. Mojtaba and H.K. Amir: J. Mater. Eng. Perform. **26** (2017) 3516–3530.
12) Z.Y. Ma, S.R. Sharma and R.S. Mishra: Metall. Mater. Trans. A **37** (2006) 3323–3336.
13) S.B. Aziz, M.W. Dewan, D.J. Huggett, M.A. Wahab, A.M. Okeil and T.W. Liao: Acta Metall. Sin. (Engl. Lett.) **29** (2016) 869–883.
14) A.G. Rao, B.R.K. Rao and V.P. Deshmukh: Mater. Lett. **63** (2009) 2628–2630.
15) P.R. Guru, F. Khan, S.K. Panigrahi and G.D.J. Ram: J. Manuf. Process. **18** (2015) 67–74.
16) H.J. Liu and X.L. Feng: Mater. Des. **47** (2013) 101–105.
17) M. Nakai, M. Niinomi, Y. Ishida, H.H. Liu, H. Fujii and T. Ninomiya: Mater. Trans. **58** (2017) 1223–1226.
18) H.C. Chen, F.Y. Hung, T.S. Lui and L.H. Chen: Mater. Trans. **58** (2017) 6–10.
19) Y. Birol and S. Kasman: Mater. Sci. Technol. **29** (2013) 1354–1362.
20) Z.Y. Ma, R.S. Mishra and M.W. Mahoney: Symposium on Friction Stir Welding and Processing II, (San Diego, 2003) pp. 221–230.
21) P. Xue, X.X. Zhang, L.H. Wu and Z.Y. Ma: Acta. Metall. Sin. **52** (2016) 1222–1238.
22) S.K. Singh, R.J. Immanuel, S. Babu, S.K. Panigrahi and G.D.J. Ram: J. Mater. Process. Technol. **236** (2016) 252–262.
23) Y.S. Sato, H. Kokawa, M. Enomoto and S. Jogan: Metall. Mater. Trans. A **30** (1999) 2429–2437.
24) D.H. Bratland, Ø. Grong, H. Shercliff, O.R. Myhr and S. Tjøtta: Acta Mater. **45** (1997) 1–22.
25) G.R. Cui, D.R. Ni, Z.Y. Ma and S.X. Li: Metall. Mater. Trans. A **45** (2014) 5318–5331.
26) M.M. El-Rayes and E.A. El-Danaf: J. Mater. Process. Technol. **212** (2012) 1157–1168.
27) E.A. El-Danaf and M.M. El-Rayes: Mater. Des. **46** (2013) 561–572.
28) S. Meenia, F. Khan, S. Babu, R.J. Immanuel, S.K. Panigrahi and G.D.J. Ram: Mater. Charact. **113** (2016) 134–143.
29) I. Gutierrez-Urrutia, M.A. Muñoz-Morris, I. Puertas, C. Luis and D.G. Morris: Mater. Sci. Eng. A **475** (2008) 268–278.
30) A.M. Kliauga and M. Ferrante: Acta Mater. **53** (2005) 345–356.
31) T. Richeton, G.F. Wang and C. Fressengeas: J. Mech. Phys. Solids **59** (2011) 2023–2043.
32) S. Sarkar, S. Mohan and S.C. Panigrahi: J. Reinf. Plastic Comp. **27** (2008) 1177–1187.